metals

MDPI

Article

Plasma Electrolytic Oxidation of Al-Zn-Mg-Ni-Fe "Nikalin" Alloys

Nikolay V. Letyagin [1,2,*], Torgom K. Akopyan [1,2], Alexander A. Sokorev [3], Ivan V. Shkaley [4], Stanislav O. Cherkasov [2], Vitali V. Doroshenko [1], Tatiana A. Sviridova [5] and Alexander Yu. Churyumov [6]

1 Sector of Scientific Activity, Moscow Polytechnic University, 38, Bolshaya Semyonovskaya str., Moscow 107023, Russia; nemiroffandtor@yandex.ru (T.K.A.); v.doroshenko@mail.ru (V.V.D.)
2 Department of Metal Forming, National University of Science and Technology MISIS, Leninsky Pr. 4, Mocow 119049, Russia; ch3rkasov@gmail.com
3 Casting Department, National University of Science and Technology MISIS, Leninsky Pr. 4, Moscow 119049, Russia; sokorev.a@misis.ru
4 Ishlinsky Institute for Problems in Mechanics RAS, Moscow 119526, Russia; ioann_shiva@list.ru
5 Institute of New Materials and Nanotechnology, National University of Science and Technology MISIS, Leninsky Prospekt 4, Moscow 119049, Russia; tim-17@yandex.ru
6 Department of Physical Metallurgy of Non-Ferrous Metals, National University of Science and Technology MISIS, Leninsky Prospekt 4, 119049 Moscow, Russia; churyumov@misis.ru
* Correspondence: n.v.letyagin@gmail.com

Abstract: Ceramic coatings were formed on the surface of as-cast Al5.2Zn1.7Mg0.4Ni0.3Fe and heat-treated Al7.0Zn2.7Mg0.5Ni0.4Fe "nikalin" aluminum alloys by using the plasma electrolytic oxidation (PEO) technique in a silicate–alkaline electrolyte. Uniform coatings containing a minimum number of defects and consisting predominantly of a γ-Al_2O_3 phase were synthesized on the surface of both Al-Zn-Mg-Ni-Fe alloys. The coatings had a microhardness of 660–1200 HV, which is 3.5–11 times higher than that of the "bare" as-cast and heat-treated alloy. The coating on the Al5.2Zn1.65Mg0.4Ni0.3Fe alloy had the highest peak hardness, which is probably caused by the lower residual alloying elements Zn and Mg in the coating bulk. As a consequence, the PEO coating with the highest hardness synthesized on the as-cast alloy exhibited a lower wear rate as compared to the heat-treated alloy. The polarization curves in 3.5% NaCl show that the PEO coatings in all cases reduced the corrosion current density and shifted the corrosion potential toward positive values, thus indicating protective properties of the coatings. The corrosion rate of the as-cast and heat-treated Al-Zn-Mg-Ni-Fe alloys increased noticeably by about 3.7–5.7 times after PEO treatment. A relationship between the residual alloying elements Zn and Mg in the bulk of the PEO coatings and corrosion resistance was established.

Keywords: Al-Zn-Mg-Ni-Fe alloys; casting alloys; plasma electrolytic oxidation (PEO); coatings; microhardness; XRD analysis; electrochemical behavior; wear resistance

Citation: Letyagin, N.V.; Akopyan, T.K.; Sokorev, A.A.; Shkaley, I.V.; Cherkasov, S.O.; Doroshenko, V.V.; Sviridova, T.A.; Churyumov, A.Y. Plasma Electrolytic Oxidation of Al-Zn-Mg-Ni-Fe "Nikalin" Alloys. *Metals* **2024**, *14*, 680. https://doi.org/10.3390/met14060680

Academic Editor: Guosong Wu

Received: 30 April 2024
Revised: 28 May 2024
Accepted: 5 June 2024
Published: 7 June 2024

1. Introduction

In the realm of commercial aluminum alloys, the 7xxx series alloys stand out for their notable attributes: a high strength-to-weight ratio, commendable ductility, formability, and exceptional corrosion resistance in various environments. At the same time, a significant issue with these alloys is their high hot-tearing tendency during casting coupled with their bad fluidity, fraction and size of eutectic and intermetallic phases, as well as macro- and micro-segregation [1]. However, recent studies of these alloys show that the addition of eutectic-forming elements, such as Ni [2,3] and Ca [4], improves the casting properties due to an increase in the fraction of eutectic phases (Al_3Ni and $(Al,Zn)_4Ca$, respectively). Furthermore, these additives promote the formation of phase compositions which significantly increase the permissible concentration of iron impurities in the alloy due to the formation of compact eutectic crystals of the Al_9FeNi and $Al_{10}CaFe_2$ phases [2–7]. A striking example of the implementation of the above approach is the design of new high-tech alloys named

"nikalin" [2,6]. These are high-strength Al-Zn-Mg-Ni-Fe system alloys which can be used in more conventional applications (casting [2,3], rolling [5,6], etc.) and even in additive technologies [7] as a substitute for commonly used alloys.

New 7xxx aluminum alloys with minor contents of eutectic-forming elements (0.5 wt.% Ni and 0.3 wt.% Fe) are investigated as promising aluminum alloy candidates that combine excellent mechanical properties with good castability [2,3]. In terms of this concept, two new modifications of the "nikalin" alloy can be distinguished. The first casting modification includes Al-Zn-Mg-Ni-Fe system alloys combining an aluminum matrix similar in composition to medium-strength self-hardening wrought 7005 alloy with a eutectic component formed by the Al_9FeNi intermetallic compound. The second modification is a high-strength casting alloy (optimized composition of 7075 alloy) differing from the former one by a higher content of Zn and Mg which allow for precipitation hardening during heat treatment. Thus, the Al6.3Zn2.1Mg0.4Fe0.6Ni alloy demonstrates improved casting properties, high mechanical properties in the as-cast state (σ_B > 450 MPa), and good mechanical properties in the deformed state (σ_B > 550 MPa). Through analogy with this alloy, the development of alloys containing calcium and iron additions as the main alloying elements is also promising [4].

However, since the development of the new Al-Zn-Mg-Ni-Fe system alloy, increasing the service life of products made of these alloys has been a promising area of research (including the formation of coatings on their surface). Functional protective coatings formed on aluminum alloy products through plasma electrolytic oxidation (PEO) widely broaden their applications and substantially increase the hardness and wear and corrosion resistance of alloy products [8–10]. Moreover, the significant advantages of this process are high productivity (the synthesis of coatings is carried out in the range of 30–40 min) and environmental friendliness, provided by the use of alkaline water-based electrolytes [11–13]. This process is widely applied in various industries, including the production of PEO-coated aluminum details for the oil and gas sector [14], moving mechanisms for marine applications [15], aircraft engineering [16], and the automotive industry [17], demonstrating its versatility and effectiveness across multiple fields.

Alloying elements, electrolyte composition, and electrical parameters determine the build-up process, quality, and performance of PEO coatings [18–21]. Studies of the microstructure and functional properties of PEO coatings on commercial alloys show that greater hardness and scratch, wear, and corrosion resistance are ascribed to the α-Al_2O_3/γ-Al_2O_3 ratio in the coatings, the lower residual alloying elements, and the thick and dense inner layer [22–24]. Moreover, analysis of the binary alloys shows that the phase composition and the morphology of the phases have a significant effect on the above properties [25–35]. Considering the influence of the main alloying elements of the 7xxx series alloys on the structure and properties of the coatings [23,24,31–34], one can conclude that Mg favors the increase in the PEO coating thickness, whereas Cu and Zn decelerate the coating formation process [23,24]. Zn, Mg, and Mn inhibit the formation of α-Al_2O_3, leading to a decrease in the hardness and wear and corrosion resistance of the coatings. The porosity of the coatings increases with the alloying element concentration (Cu, Mg), this being additional evidence that residual alloying elements have a negative effect on the corrosion properties of the coatings [31–35].

The promising potential of nickel alloying of aluminum alloys originates from the relatively large volume fraction of fine-morphology eutectic Al_3Ni or Al_9FeNi phases (in the presence of Fe as the main alloying element in the aluminum alloys) forming during solidification and allowing for the good technological and mechanical properties of the alloys. This was reported in a number of publications and attracted great attention, especially for potential high-temperature applications [36–38]. However, the issue of PEO coating formation on such alloys, in particular those with high-alloyed aluminum matrices such as the Al-Zn-Mg-Ni-Fe alloys, has not been studied yet. The results of a few known studies show that Ni as an alloying element contributes to the formation of PEO coatings with an increased fraction of γ-Al_2O_3 and decreases the microhardness and thickness of

the coatings [18]. The corrosion resistance of the coated samples decreases with an increase in the Ni content in the matrix, while the anti-wear performance of the treated samples is improved [39].

However, an analysis of the scientific literature shows that to date, there are no reports devoted to the study of the features of PEO coatings formed on new high-tech Al-Zn-Mg-Ni-Fe alloys. In this work, the microstructures, phase compositions, mechanical properties, and corrosion and wear resistances of casting Al-Zn-Mg-Ni-Fe alloys and PEO coatings were investigated systematically.

2. Materials and Methods

Two model alloys, i.e., Al5.2Zn1.7Mg0.4Ni0.3Fe and Al7.0Zn2.7Mg0.5Ni0.4Fe, were selected for a comparison of coatings formed through plasma electrolytic oxidation. The alloys were prepared from technical purity aluminum (99.7%) in a resistance furnace. The selected compositions were prepared from pure Zn, Mg, and an Al-20% Ni binary master alloy. After the melting of the basic components, the metal was cast into a graphite mold with a working cavity with a diameter of 40 mm and a depth of 180 mm at 780–800 °C.

The billet Al7.0Zn2.7Mg0.5Ni0.4Fe alloy was subjected to two-stage homogenizing annealing at 450 and 540 °C with a duration of 3 h in each stage, the expedience of which was reported earlier [6]. The last stage of the process was a hardening heat treatment in mode T1 (quenching plus artificial aging for maximum strength at 140 °C with a duration of 6 h).

The billets were mechanically processed by cutting them for further coating formation.

The coatings were formed using a PEO installation with a 250 kW high-frequency high-voltage switching power supply unit. The PEO process was conducted in a silicate–alkaline electrolyte containing 2 g/L KOH, 6 g/L Na_2SiO_3, and 1 g/L H_3BO_3 in distilled water. The electrolyte was homogenized through stirring, and its temperature near the electrolyte cell was kept at 15–20 °C during PEO coating deposition. The following electrical parameters were maintained during coating formation: anode voltage U_a = 1000 V; cathode voltage U_k = 300 V; current density 25 A/dm^2; pulse frequency f = 3 kHz. The PEO process duration was 30 min.

Thermodynamic calculations, including the determination of the volume fractions of the solid phases and the fracture as functions of temperature in the interval of nonequilibrium and equilibrium solidification, were performed using the Thermo-Calc software version 5 (TTAL5 database).

Scanning electron microscopy (SEM; TESCAN VEGA 3, Brno, Czech Republic) and electron microprobe analysis (EMPA; OXFORD AZtec, Oxford Instruments, Oxfordshire, UK) were employed to examine the morphology and elemental compositions of the surfaces and cross-sections of the PEO coatings. X-ray diffraction (XRD) data were obtained at room temperature using a DRON-4 diffractometer (Burevestnik Innovation Centre, St. Petersburg, Russia) in Co Kα radiation and analyzed with a software package [40]. XRD profiles were taken in a 2θ range from 10 to 130 deg with a 0.1 deg step and a 3 s exposure.

Microhardness measurements were conducted using DUROLINE MH-6 (Metkon, Bursa, Turkey). The Vickers indentation loads were 50 g, with the dwell time being 5 s.

The dry sliding wear tests of PEO coatings were conducted using an MFT-5000 tribotester (Rtec Instruments, San Jose, CA, USA) in contact ball-on-disk setup according to ASTM G99-17 [41] under ambient conditions (23 °C, relative humidity 45–50%). A constant normal load of 10 N was applied to a 10 mm diameter ZrO_2 ceramic ball counterpart (Vickers hardness of more than 1220 HV). The wear track radius was set to 14.5 mm. The rotating speed was 131.7 rpm (0.2 m·s^{-1}), with the sliding time being 5000 s, corresponding to a sliding distance of 1000 m.

The surface topography of the samples after testing was studied using a noncontact optical S neox 3D profilometer (SENSOFAR-TECH, Barcelona, Spain). Scanning was carried out at a reduced speed and automated stitching of single frames into one area using a 10× lens in confocal mode. The worn volume of the entire friction groove was measured from

the resulting images using the device's software. Specific wear rates were calculated by dividing the wear volume loss by the total sliding distance and load. The roughness of the original surface of the samples was evaluated in accordance with ISO 4287 [42] in some areas under the same scanning conditions (for a single frame using a 150× confocal lens).

Corrosion testing (polarization curve measurements) of alloy samples (3 different samples for each state) was carried out in a 3.5% NaCl solution by using an IPC-Pro electronic potentiostat (Volta Co. Ltd., Saint-Petersburg, Russia). The samples were polarized from the cathodic region to the anodic one at a potential sweep rate of 1 mV/s. The reference electrode was saturated $Ag/AgCl_2$, and the auxiliary electrode was platinum.

3. Results

The as-cast Al5.2Zn1.7Mg0.4Ni0.3Fe and heat-treated Al7.0Zn2.7Mg0.5Ni0.4Fe alloys were processed using the PEO technology. The actual chemical composition (wt.%) and Vickers hardness (HV) of the alloys are presented in Table 1.

Table 1. Actual chemical composition (wt.%) and Vickers hardness (HV) of alloys.

No	Alloy	Actual Chemical Composition, wt.%						HV
		Al	Zn	Mg	Ni	Fe	Si	
1	Al5.2Zn1.7Mg0.4Ni0.3Fe	balance	5.2	1.7	0.4	0.3	0.04	108
2	Al7.0Zn2.7Mg0.5Ni0.4Fe	balance	7.0	2.7	0.6	0.4	0.06	182

The as-cast Al5.2Zn1.7Mg0.4Ni0.3Fe alloy (Figure 1a,c) consists of Al dendritic cells surrounded by an equilibrium eutectic Al_9FeNi phase. According to the calculated data (Figure 2), nonequilibrium T ($Al_2Mg_3Zn_3$) phase inclusions can also be observed. However, the fraction of T ($Al_2Mg_3Zn_3$) phases of crystallization origin is insignificant (microstructural analysis did not reveal them). Zn and Mg in the Al-Zn-Mg matrix are designed to improve the mechanical properties due to the natural formation of a secondary phase from the supersaturated solid solution obtained after casting.

The temperature dependence of the mole fraction of the solid phases in the solidification range calculated using the Scheil–Gulliver model (Figure 2) suggests that the solidification of the Al7.2Zn2.7Mg0.5Ni0.4Fe alloy is completed by the eutectic reaction $L \rightarrow (Al) + Al_9FeNi + T$ at 482.5 °C. As a result of this reaction, the nonequilibrium T ($Al_2Mg_3Zn_3$) phase forms and binds to a significant part of zinc and magnesium. Therefore, homogenizing annealing of the castings for dissolution of the nonequilibrium T phase and subsequent hardening heat treatment (quenching plus artificial aging) was carried out.

The final structure of the self-hardening Al5.2Zn1.7Mg0.4Ni0.3Fe alloy (Figure 1a,c) and heat-treated (after quenching and aging) Al7.2Zn2.8Mg0.5Ni0.4Fe (Figure 1b,d) alloy consists of the aluminum matrix (Al), eutectic Al_9FeNi particles, and M ($MgZn_2$) precipitates (Figure 3). According to the thermodynamic calculations (Thermo-Calc software), the volume fraction of the Al_9FeNi phase is approximately 2.5% in both alloys, which is confirmed by the XRD data. However, the volume fraction of the M phase in the heat-treated Al7.2Zn2.7Mg0.5Ni0.4Fe (~10.9%) alloy is significantly higher compared to the self-hardening Al5.2Zn1.7Mg0.4Ni0.3Fe (~7.5%) alloy.

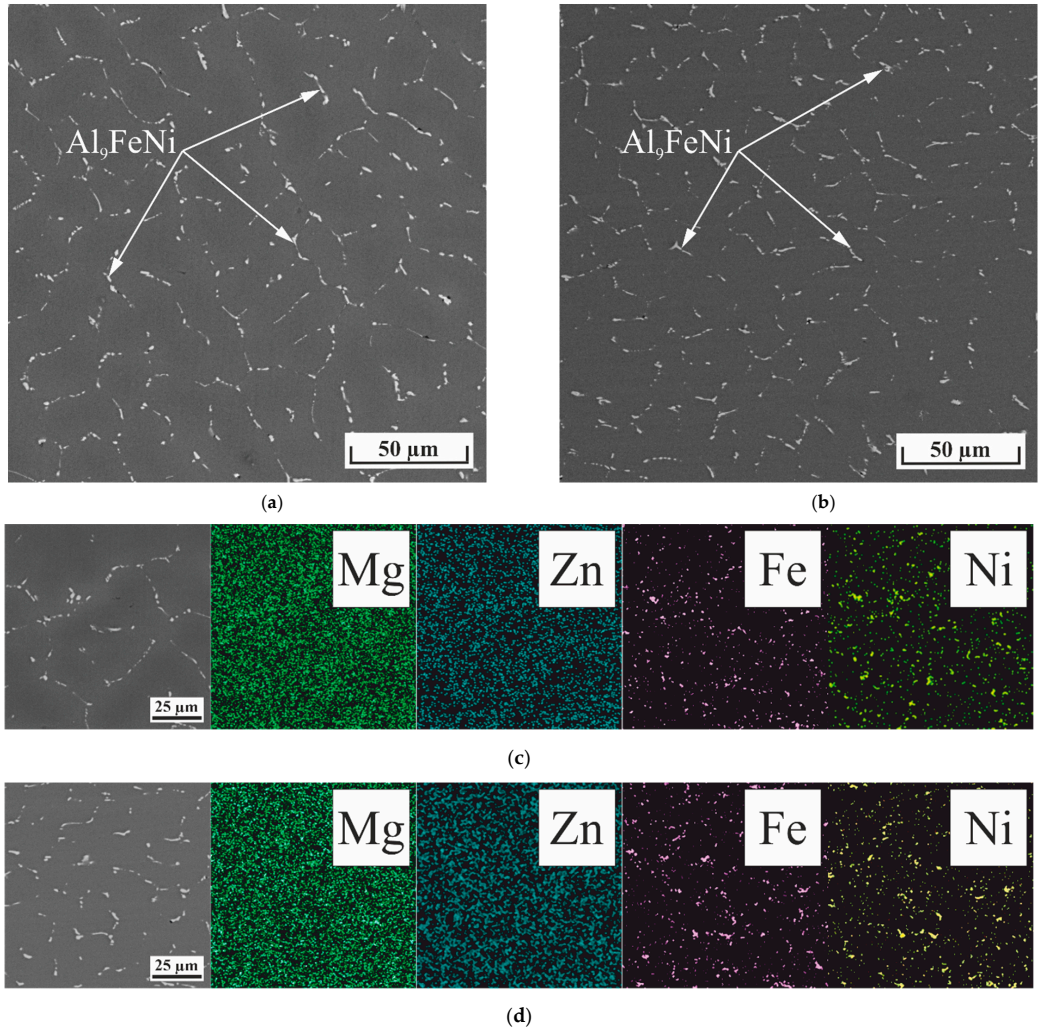

Figure 1. Microstructure and element distribution maps of (**a**,**c**) as-cast Al5.2Zn1.7Mg0.4Ni0.3Fe and (**b**,**d**) heat-treated Al7.2Zn2.8Mg0.5Ni0.4Fe alloys.

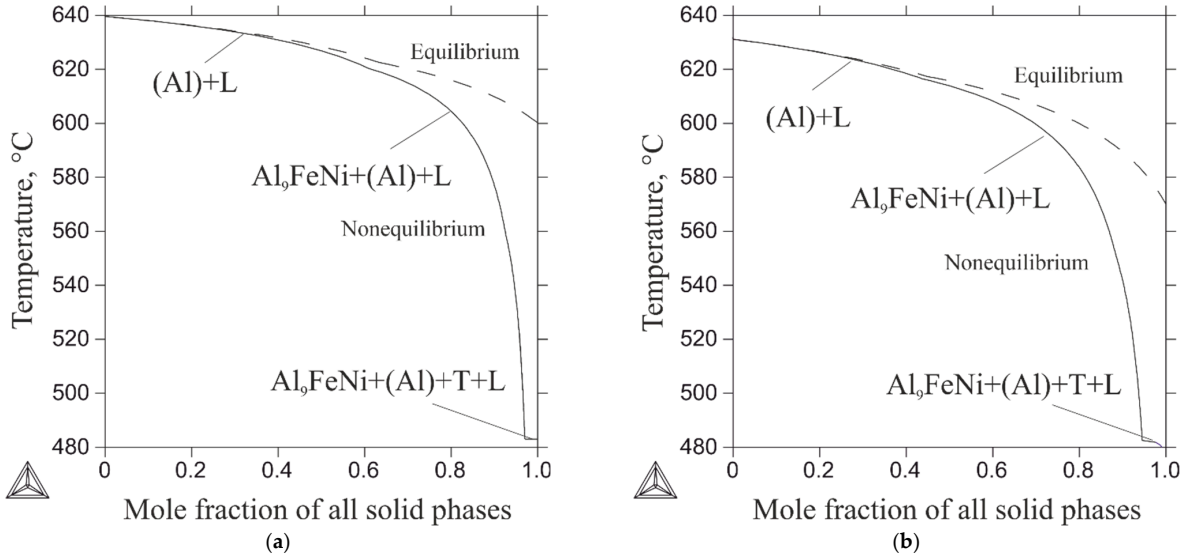

Figure 2. Temperature dependence of mole fraction of solid phases upon nonequilibrium solidification of (**a**) Al5.2Zn1.65Mg0.4Ni0.3Fe and (**b**) Al7.2Zn2.8Mg0.5Ni0.4Fe alloys (Thermo-Calc software).

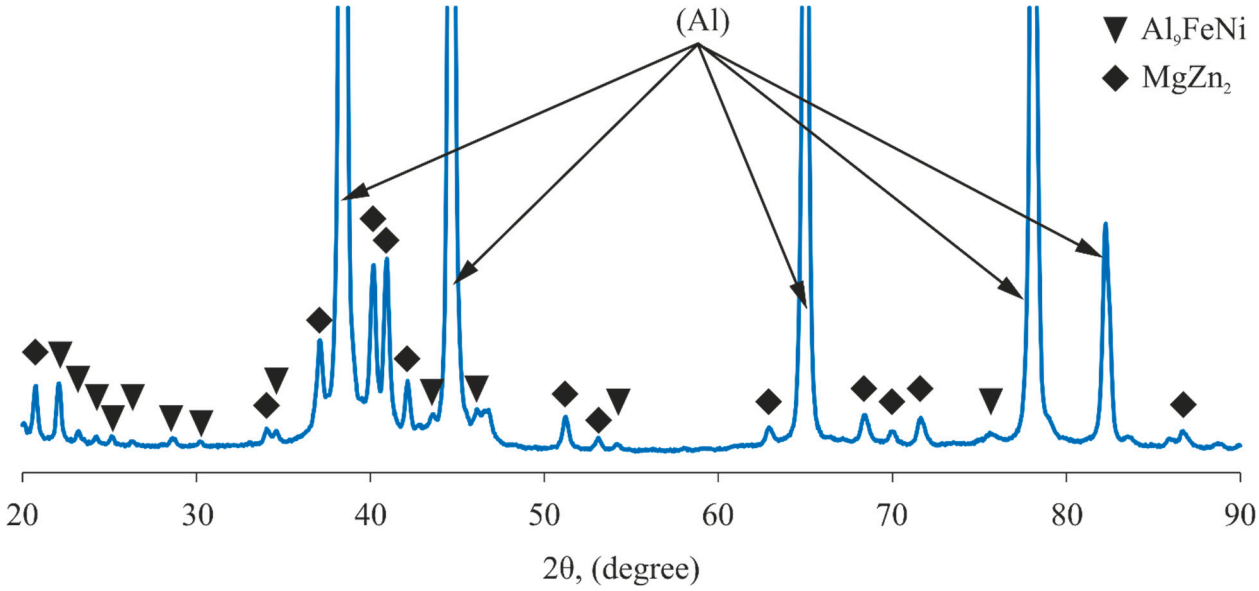

Figure 3. Results of XRD analysis of heat-treated Al7.0Zn2.7Mg0.5Ni0.4Fe alloy.

The difference in the chemical compositions of the alloys and specific post-processing conditions (including heat treatment) allows for the precipitation hardening of the alloys with the formation of different volume fractions of second phases. As a result, the hardness values of the as-cast Al5.2Zn1.7Mg0.4Ni0.3Fe 108 HV alloy and that of the heat-treated Al7.0Zn2.7Mg0.5Ni0.4Fe 182 HV alloy differ significantly (Table 1).

Thus, in addition to the good mechanical properties of the new casting alloys and their relatively good manufacturability in the casting process [2,3], it is of particular interest to compare the prospects of PEO coatings formed on these alloys for increasing the hardness, wear resistance, and corrosion resistance of the alloys.

3.1. Surface and Cross-Sectional Microstructure of PEO Coatings

Figure 4 presents a comparison of the surface topography of the PEO-coated samples, evaluated by using confocal profilometry. The main surface roughness parameters Ra and Rz [17] are summarized in Table 2. It is evident that the two PEO-treated alloys exhibit equal roughness. These data confirm the generally similar appearance of the surface topographies of the oxide layers grown on the alloys.

Table 2. Average roughness values (Ra and Rz) of PEO-treated alloys; thickness of oxide layers on PEO-treated alloys.

No	Alloy	Surface Roughness, μm		Thickness of Oxide Layer, μm
		Ra	Rz	
1	Al5.2Zn1.65Mg0.4Ni0.3Fe	2.6	18.2	50
2	Al7.0Zn2.7Mg0.5Ni0.4Fe HT	2.2	17.4	58

The thickness of the coating as measured through image analysis from the SEM micrographs is 50 ± 2 μm for the as-cast substrate of the Al5.2Zn1.65Mg0.4Ni0.3Fe alloy and 58 ± 2 μm for the heat-treated Al7.0Zn2.7Mg0.5Ni0.4Fe one (Table 2, Figure 5a,b).

The coatings grown on the aluminum alloys exhibit the highest uniformity. No external crater-like pores which are typical of PEO coatings are identified. The inner coating layer is dense and has no scattered porosity. The interfaces between the oxide layer and the base metal are regular, indicating a neutral effect of the Al_9FeNi phase on the coating growth kinetics.

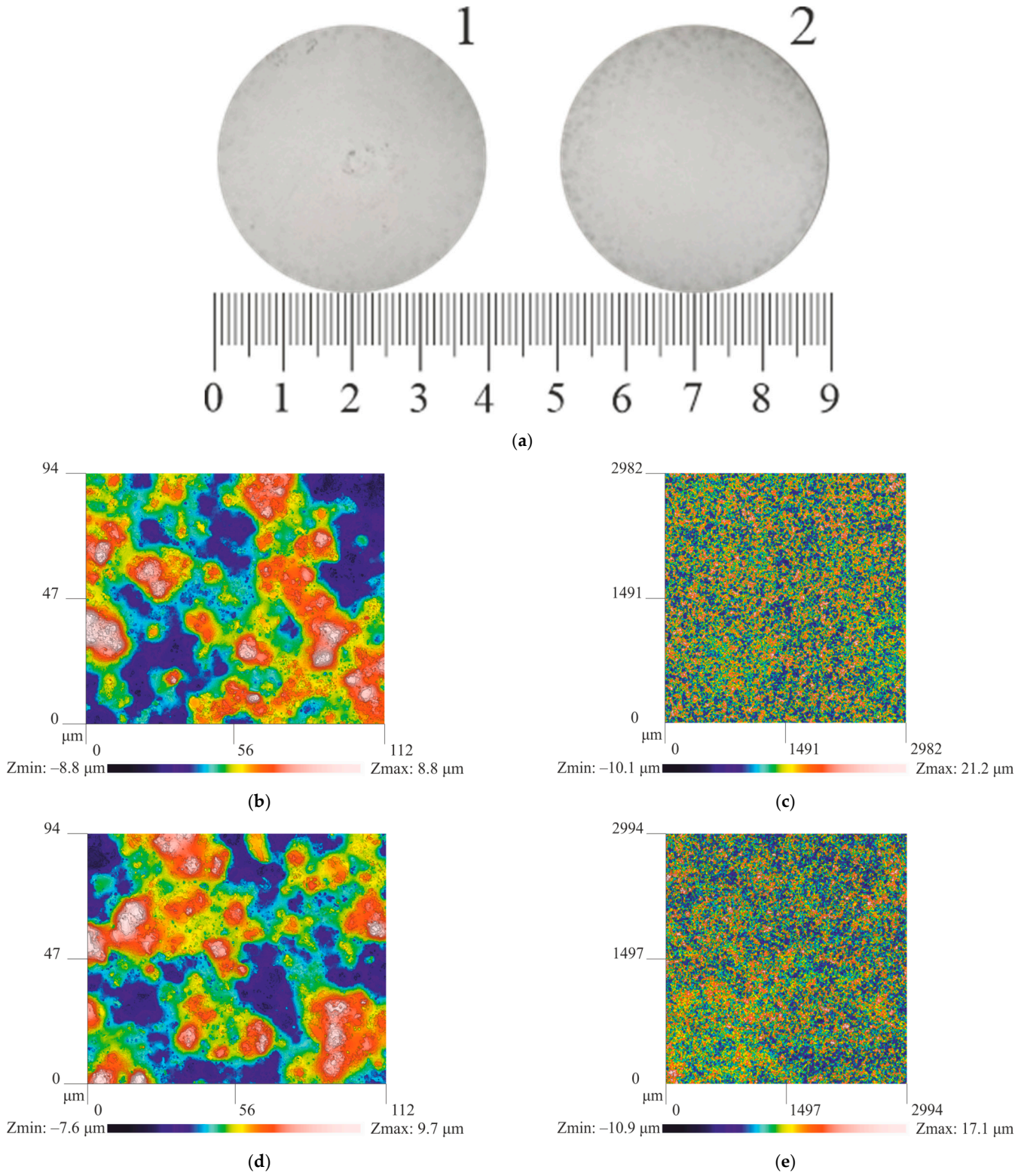

Figure 4. (**a**) Appearance of aluminum substrates with PEO coatings synthesized in base electrolyte for 30 min; surface topography, analyzed by using confocal profilometry, of (**b**,**c**) as-cast Al5.2Zn1.65Mg0.4Ni0.3Fe (1), (**d**,**e**) heat-treated Al7.0Zn2.7Mg0.5Ni0.4Fe (2) PEO-coated samples.

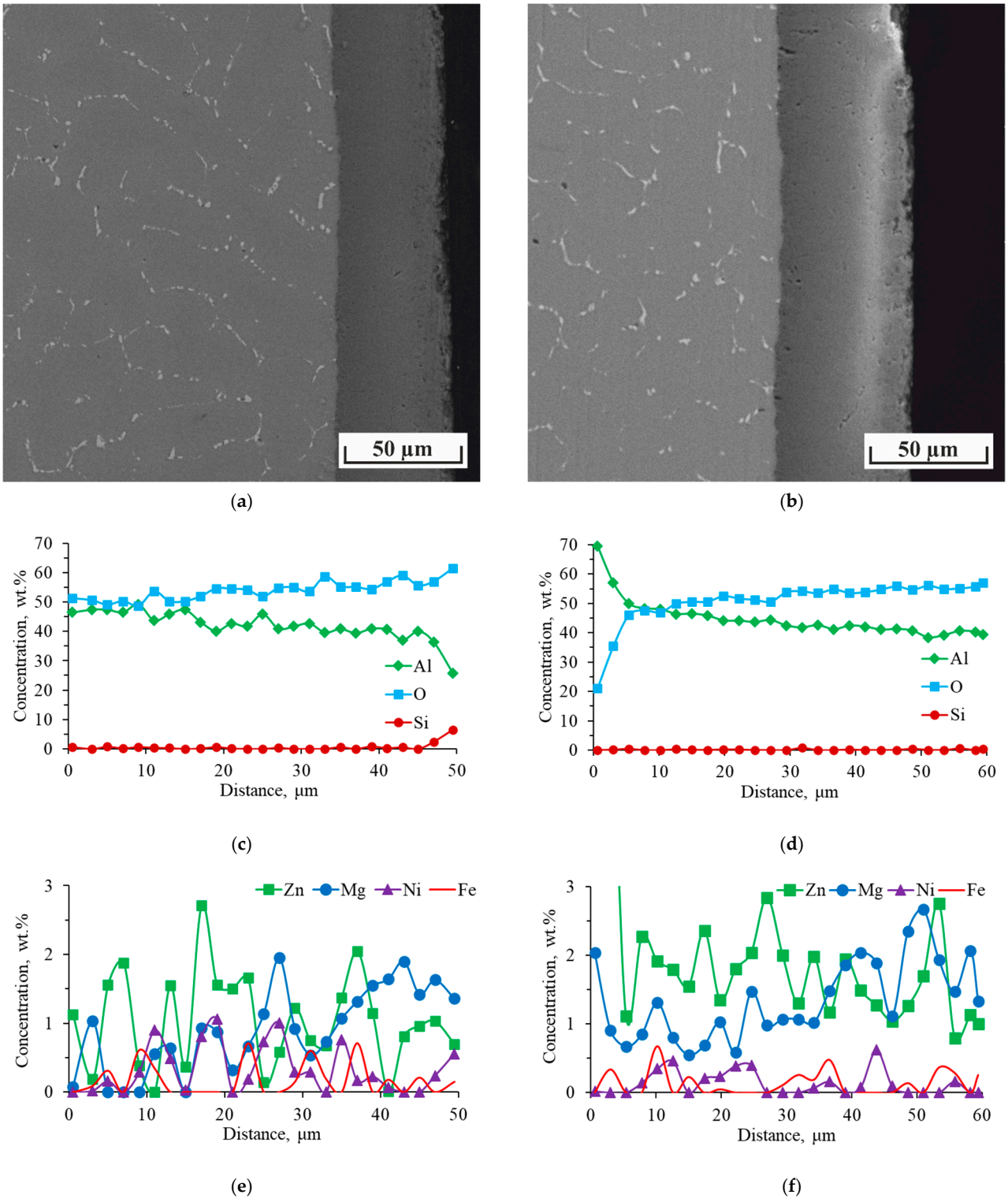

Figure 5. Cross-sectional distribution of main elements in PEO coatings formed on various aluminum substrates: (**a**,**c**,**e**) as-cast Al5.2Zn1.65Mg0.4Ni0.3Fe and (**b**,**d**,**f**) heat-treated Al7.0Zn2.7Mg0.5Ni0.4Fe.

Figure 5c–f show the cross-sectional distribution of the main elements between the substrate and the PEO coating. It can be seen that the distribution of aluminum and oxygen over the thickness of the PEO layers is relatively stable up to the coating surface, where there is a simultaneous decrease in aluminum content and an increase in silicon content (Figure 5c). Also, the main elements of the alloys present in the substrates are Zn and Mg

(Figure 5e,f). Moreover, it is worth noting that the increased Zn and Mg contents in the substrate (Figure 5e,f) increase their content in the coating. Thus, the average Zn content in the coating bulk increases from 1.2 to 1.65%, and the magnesium content increases from 0.9 to 1.55% with an increase in the Zn and Mg contents in the alloys. It is also noteworthy that the nickel content in the coating formed on the as-cast alloy (Figure 5e) is higher than that in the coating formed on the heat-treated alloy (Figure 5f), despite its lower content in the former alloy. The average Ni contents in the coatings are 0.2 and 0.1%, respectively. The Fe content in both coatings is almost at the same level, ~0.1%.

Based on the XRD data (Figure 6), the PEO coatings on both aluminum alloys mainly consist of γ-Al_2O_3. The volume fractions of γ-Al_2O_3 are about 99%.

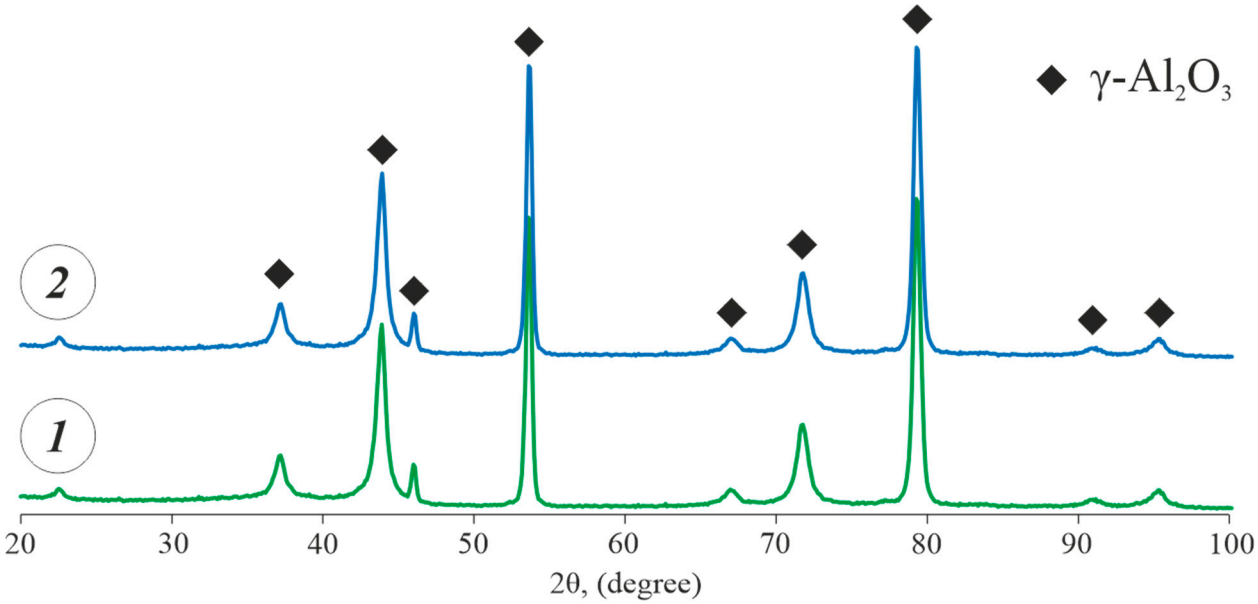

Figure 6. XRD patterns of PEO coatings grown on various aluminum substrates: (1) as-cast Al5.2Zn1.7Mg0.4Ni0.3Fe and (2) heat-treated Al7.0Zn2.7Mg0.5Ni0.4Fe.

3.2. Microhardness of PEO Coatings

The microhardness of the central part of the polished coating samples in the cross-section was measured (Figure 7). The average microhardness of the coatings formed on the as-cast Al5.2Zn1.7Mg0.4Ni0.3Fe substrates is 954 (690–1200 HV range) (Table 3). The coatings formed on the heat-treated Al7.0Zn2.7Mg0.5Ni0.4Fe substrates exhibit a lower average hardness of 825 HV (660–1040 HV range). Despite the influence of the substrate on the hardness of the coatings, the formation of the coatings significantly increases the hardness of the alloy surface. The microhardness of the «bare» as-cast and heat-treated "nikalin" alloys are about 108 and 182, respectively.

Table 3. The average microhardness (min–max) in the central part of the coating thickness.

Alloy	Microhardness, HV
Al5.2Zn1.65Mg0.4Ni0.3Fe	954 (690–1200)
Al7.0Zn2.7Mg0.5Ni0.4Fe	825 (660–1040)

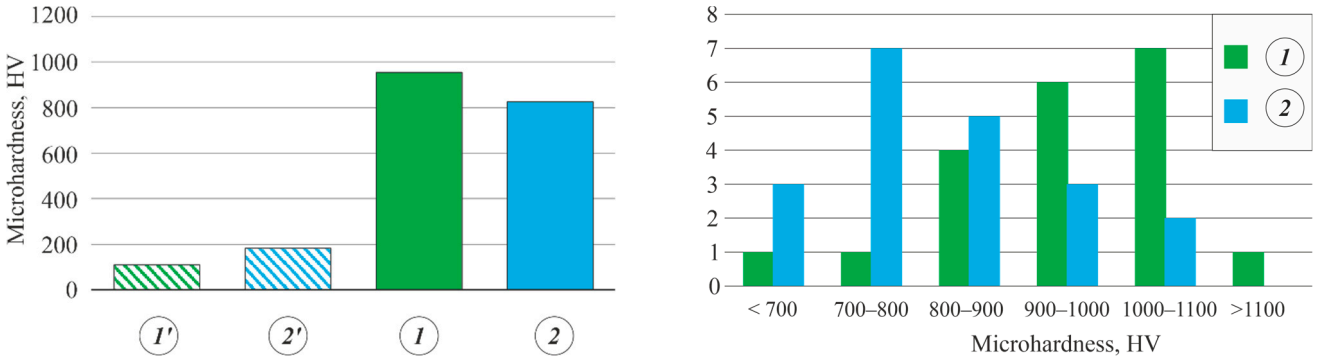

(**a**) (**b**)

Figure 7. (**a**) Average microhardness of alloys for "bare" (*1′*) as-cast Al5.2Zn1.7Mg0.4Ni0.3Fe and (*2′*) heat-treated Al7.0Zn2.7Mg0.5Ni0.4Fe alloys and for PEO-coated (*1*) Al5.2Zn1.7Mg0.4Ni0.3Fe and (*2*) Al7.0Zn2.7Mg0.5Ni0.4Fe alloys; (**b**) hardness distribution histogram at half-thickness of PEO coating.

3.3. Wear Resistance

The friction coefficient of the PEO coatings was recorded throughout the experiment as a function of test time. It can be seen from Figure 8 that the friction coefficient of the PEO coatings is in the 0.8–0.88 range. The friction coefficient variation for the PEO coatings exhibits periodic fluctuations and a smooth curve. The friction coefficient grows to 0.88 during the first 3–4 min. This period can be considered run-in mode. Then, a constant friction coefficient is established until the end of the test at 0.8 for the PEO coating formed on the as-cast alloy and 0.82 for the heat-treated one (Table 4).

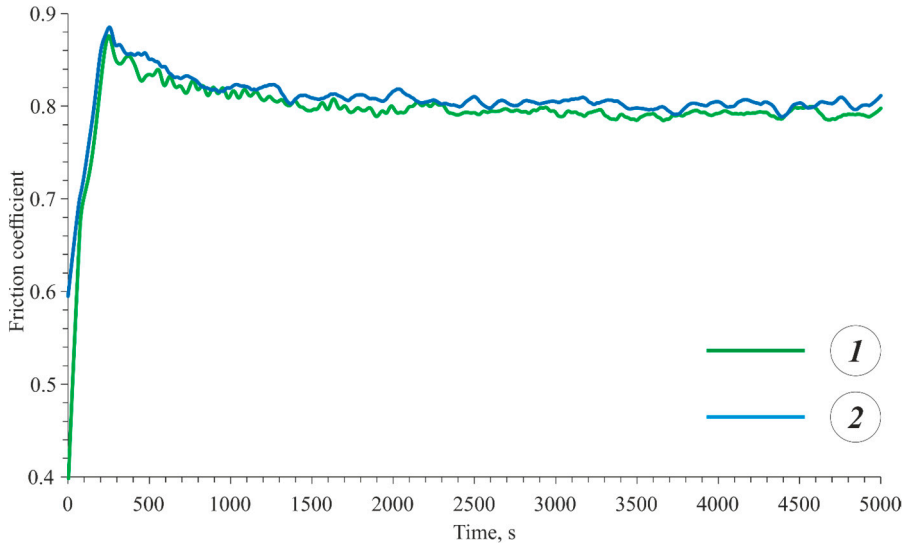

Figure 8. Dependence of friction coefficient on test time under load of 10 N for PEO coatings formed on (*1*) as-cast Al5.2Zn1.65Mg0.4Ni0.3Fe and (*2*) heat-treated Al7.0Zn2.7Mg0.5Ni0.4Fe.

Table 4. Data on wear rates of PEO coatings formed on as-cast Al5.2Zn1.65Mg0.4Ni0.3Fe and heat-treated Al7.0Zn2.7Mg0.5Ni0.4Fe alloys.

Sample	Coefficient of Friction	Wear Rate ($mm^3/N \cdot m$)
as-cast Al5.2Zn1.65Mg0.4Ni0.3Fe + PEO	0.8	2.36×10^{-4}
heat-treated Al7.2Zn2.8Mg0.5Ni0.4Fe + PEO	0.82	2.57×10^{-4}

Figure 9 shows the cross-sectional profile of the wear track for the PEO coatings formed on "nikalin". The PEO coating formed on the as-cast alloy exhibits a higher wear resistance (wear rate is 2.36 × 10^{-4} mm^3/N·m) compared to the heat-treated alloy (wear rate is 2.57 × 10^{-4} mm^3/N·m) (Table 4).

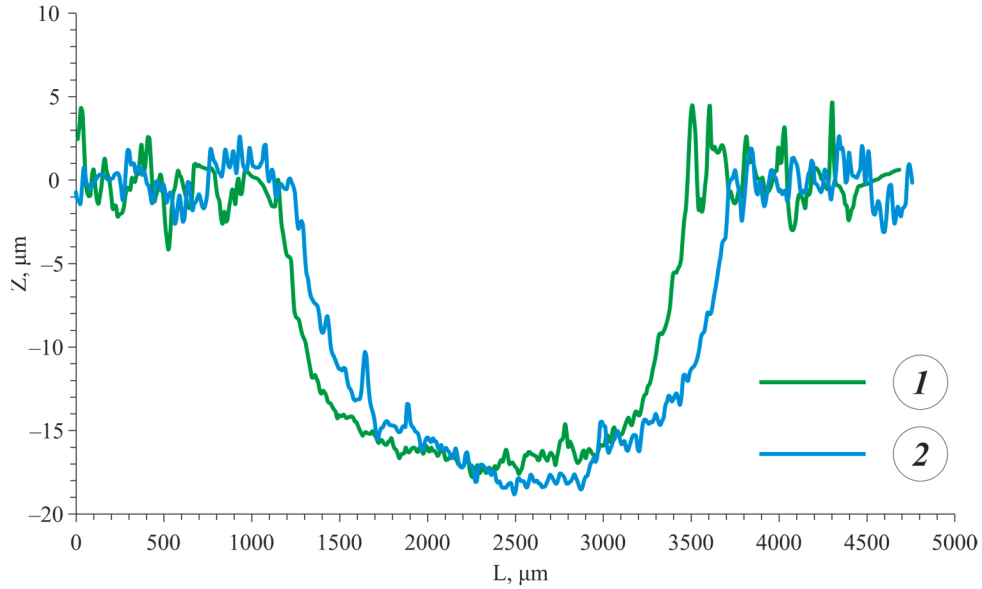

Figure 9. Cross-sectional profiles of wear track after wear tests under load of 10 N for PEO coatings formed on (*1*) as-cast Al5.2Zn1.65Mg0.4Ni0.3Fe and (2) heat-treated Al7.0Zn2.7Mg0.5Ni0.4Fe.

3.4. Electrochemical Behavior of PEO Coatings

Figure 10 shows the polarization diagrams of the test Al alloys. The effect of alloying elements (Zn and Mg) on the corrosion resistance of the PEO coatings and the corrosion current densities (Icorr) are determined through polarization curve extrapolation and corrosion potential (Ecorr) measurements. Table 5 summarizes Icorr and Ecorr for the test samples. It can be seen that increasing the share of Zn and Mg addition to the Al-Zn-Mg-Ni-Fe system leads to an increase in the corrosion current density (Icorr) as compared to that of Al5.2Zn1.7Mg0.4Ni0.3Fe (45.1 × 10^{-3} and 14.9 × 10^{-3} mA/cm^2, respectively).

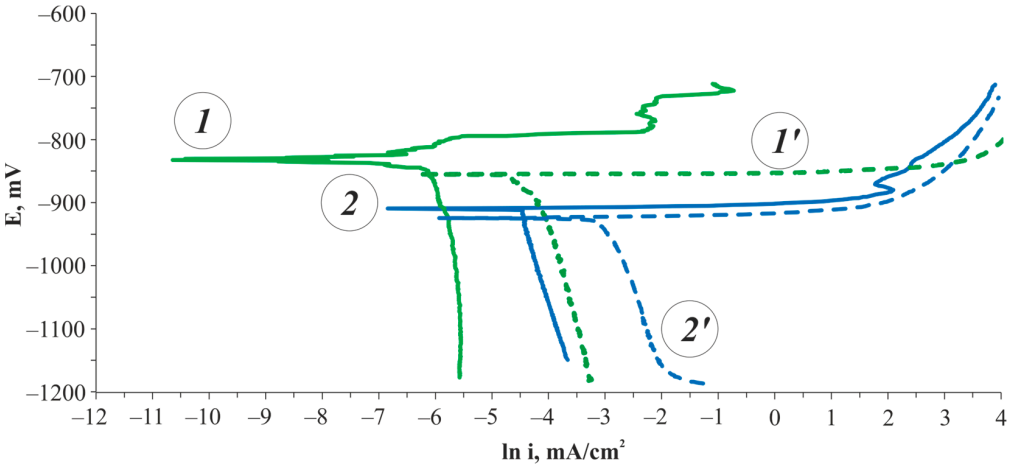

Figure 10. Polarization dependences of current density, lni, on potential E in 3.5% NaCl solution at potential sweep rate of 1 mV/s for "bare" (*1′*) as-cast Al5.2Zn1.7Mg0.4Ni0.3Fe and (*2′*) heat-treated Al7.0Zn2.7Mg0.5Ni0.4Fe alloys and for PEO-coated (*1*) Al5.2Zn1.7Mg0.4Ni0.3Fe and (2) Al7.0Zn2.7Mg0.5Ni0.4Fe alloys. Potentials are shown relative to silver chloride electrode (Ag/AgCl).

Table 5. Results of potentiodynamic corrosion tests in 3.5% NaCl solution for uncoated alloys and PEO-coated alloys.

Sample	Corrosion Potential, $E_{corr.}$ (mV)	Corrosion Current Density, $i_{corr.}$ (mA/cm^2)
as-cast Al5.2Zn1.7Mg0.4Ni0.3Fe	−860	14.9×10^{-3}
as-cast Al5.2Zn1.7Mg0.4Ni0.3Fe + PEO	−804	2.6×10^{-3}
heat-treated Al7.0Zn2.7Mg0.5Ni0.4Fe	−932	45.1×10^{-3}
heat-treated Al7.0Zn2.7Mg0.5Ni0.4Fe + PEO	−920	12.2×10^{-3}

Polarization curve analysis (Figure 10) shows that the PEO coatings shift the steady-state electrode potential to the positive potential area in all cases. The reduced corrosion current (Table 5) and the increased corrosion potential suggest that the coatings have protective properties. Of all the tested PEO-treated alloys, the Al7.0Zn2.7Mg0.5Ni0.4Fe alloy has the highest corrosion current density (12.2×10^{-3} mA/cm^2) and therefore the lowest corrosion resistance, followed by Al5.2Zn1.65Mg0.4Ni0.3Fe (2.6×10^{-3} mA/cm^2), which has the lowest corrosion current density.

4. Discussion

The as-cast Al5.2Zn1.7Mg0.4Ni0.3Fe and heat-treated Al7.2Zn2.8Mg0.5Ni0.4Fe casting alloys with different Zn and Mg concentrations and process conditions proved to have differences in the formation and final properties of the obtained coatings. Increasing the Zn and Mg concentrations in the alloys increased the thickness of the coatings. Earlier studies [23,31] confirmed that the coating thickness increased with an increase in the Mg content in the substrates. It should be noted that the surfaces of the coatings forming on the Al-Zn-Mg-Ni-Fe alloys were quite uniform. This feature is especially important in comparison with conventional Al-Si alloys used for shaped casting [3]. For example, the presence of the eutectic phase leads to a local decrease in the coating thickness, as evidenced by the wavy interface between the oxide coating and the base metal [25,30]. In our case, the presence of a significant volume fraction (~2 wt.%) of the Al_9FeNi eutectic phase did not prevent the uniform growth of the coating.

Despite the increase in the residual Zn and Mg contents in the coatings with an increase in the Zn and Mg contents in the alloy, the Ni content decreased. This can be due to the heat-treated state of the alloy. A similar dependence was observed earlier for binary Al-Ni system alloys. The nickel-containing phase was observed only in the coating of the as-cast Al-Ni alloy [18].

Detailed analysis of the XRD results revealed that unlike the PEO coatings formed on the pure aluminum and eutectic aluminum alloys with low fractions of second phases in a silicate–alkaline electrolyte (PEO duration up to 60 min), the coatings grown on the "nikalin" substrates contained only γ-Al_2O_3. Zn, Mg, and Ni can suppress the formation of α-Al_2O_3, which is confirmed by earlier results [18,23,24].

However, despite the identified differences in the phase composition of the coatings, the dense coatings formed on the "nikalin" alloys provided the same mechanical properties as those of the coatings formed on pure Al (after similar PEO treatment). While the average microhardness of the coatings formed on pure Al was in the 740–1180 HV range [30], the growth of the γ-Al_2O_3 volume fraction in the "nikalin" alloy coating provided microhardness values of 690–1200 HV for as-cast "nikalin" and 660–1040 HV for heat-treated "nikalin". Moreover, the decrease in the hardness for the heat-treated alloys can be accounted for by the increase in the residual content of Zn and Mg coming from the coating. It is worth noting that the hardness of the coatings formed on the alloys with high concentrations of elements for the alloying of the solid solutions was significantly higher than that of the coatings formed on the eutectic alloys with a greater fraction of second phases [30].

The PEO coating formed on the as-cast alloy exhibited a higher wear resistance as compared to the heat-treated alloy due to the highest hardness of the PEO coating on the as-cast alloy.

The corrosion test results for the alloys show that the alloying elements (Zn, Mg, Ni, Fe) of the high-strength "nikalin" alloys and the phase compositions formed by these elements decrease the corrosion resistance of pure aluminum [8,30]. The corrosion potential of pure aluminum (−625 mV) shifted toward negative values, namely to −860 mV for the as-cast Al5.2Zn1.65Mg0.4Ni0.3Fe alloys. The increased Zn and Mg contents led to the formation of the M ($MgZn_2$) phase during heat treatment (quenching and annealing), which produced anodic regions shifting the corrosion potential toward more negative values (pure Al: 625 mV; heat-treated Al7.2Zn2.8Mg0.5Ni0.4Fe: −932 mV). Increasing the contents of those phases in the Al matrix led to the formation of micro-galvanic pairs [43,44] between the Al and M phases, which in turn facilitated the cathodic and anodic processes and hence increased the corrosion current density of the heat-treated Al7.2Zn2.8Mg0.5Ni0.4Fe alloy (45.1×10^{-3} mA/cm^2) in comparison with that for the as-cast Al5.2Zn1.7Mg0.4Ni0.3Fe one (14.9×10^{-3} mA/cm^2). However, it should be taken into account that in the case of the multiphase alloys considered, this interaction can be much more complicated.

The reduced corrosion current and the increased corrosion potential demonstrate the effectiveness of these PEO coatings in terms of increasing the corrosion resistance of products made of Al-Zn-Mg-Ni-Fe alloys [30]. The coatings decreased the corrosion current by about 3.7–5.7 times in comparison with that of the uncoated alloys. Moreover, the above effect was greater for the PEO coatings formed on the as-cast Al5.2Zn1.65Mg0.4Ni0.3Fe alloy. It is safe to assume that the effect on the corrosion resistance was greater for the PEO coatings formed on as-cast Al5.2Zn1.65Mg0.4Ni0.3Fe due to the lower fraction of residual Zn and Mg in the bulk of the PEO coatings.

5. Conclusions

In this study, the structure and properties of initial as-cast Al5.2Zn1.7Mg0.4Ni0.3Fe and heat-treated Al7.2Zn2.8Mg0.5Ni0.4Fe "nikalin" samples were characterized. The surfaces of aluminum alloys were treated through PEO. Each coating was studied using the characterization of the appearance, elemental distribution, phase analysis, microhardness, wear resistance, and electrochemical behavior. A comparative analysis was made for the uncoated and the PEO-treated casting alloys. The results were as follows.

(1) The as-cast and heat-treated Al-Zn-Mg-Ni-Fe alloys had compact microstructures consisting of an aluminum matrix (Al), M ($MgZn_2$) precipitates, and eutectic Al_9FeNi particles. The hardness of the casting Al5.2Zn1.7Mg0.4Ni0.3Fe and heat-treated Al7.2Zn2.8Mg0.5Ni0.4Fe alloys was 108 and 180 HV, respectively.

(2) The PEO coatings formed on the as-cast and heat-treated Al-Zn-Mg-Ni-Fe alloys in a silicate–alkaline electrolyte were uniform and contained a minimum number of defects. Their microhardness varied in the 660–1200 HV range, which was 3.6–11.1 times higher than that of the uncoated base alloys. The predominant phase in the coatings was γ-Al_2O_3.

(3) The PEO coating formed on the as-cast alloy exhibited a higher wear resistance compared to the heat-treated alloy due to the highest hardness of the PEO coating on the as-cast alloy.

(4) An increase in the fraction of the second phases in the structure of heat-treated Al7.2Zn2.8Mg0.5Ni0.4Fe led to a decrease in the corrosion resistance of the alloy in comparison with as-cast Al5.2Zn1.7Mg0.4Ni0.3Fe. The corrosion rates of the as-cast and heat-treated Al-Zn-Mg-Ni-Fe alloys increased significantly after PEO treatment by about 3.7–5.7 times. The effect on the corrosion resistance was greater for the PEO coatings formed on as-cast Al5.2Zn1.65Mg0.4Ni0.3Fe due to the lower fraction of residual Zn and Mg in the bulk of the PEO coatings.

Thus, the Al-Zn-Mg-Ni-Fe "nikalin" casting alloys have a high potential for the industrial production of high-tech products with increased strength characteristics, and the

PEO treatment performed in accordance with the modes described herein has promising potential to increase the hardness of "nikalin" alloy parts and protect the alloys from corrosion and wear.

Author Contributions: Conceptualization, N.V.L. and T.K.A.; data curation, S.O.C. and N.V.L.; investigation, A.A.S., S.O.C., I.V.S., V.V.D., T.A.S. and A.Y.C.; methodology, N.V.L. and T.K.A.; writing—original draft, N.V.L.; writing—review and editing, T.K.A. All authors have read and agreed to the published version of the manuscript.

Funding: This study was financially supported by the Moscow Polytechnic University within the framework of the grant named after Pyotr Kapitsa (SEM, EMPA, XRD, surface topography, electrochemical behavior) and by the Russian Science Foundation, grant number 23-79-00055 (HV, wear resistance).

Data Availability Statement: The original contributions presented in the study are included in the article, further inquiries can be directed to the corresponding author.

Acknowledgments: The authors would like to thank the JSC Aluminum Alloys Plant (JSC Aluminum Alloys Plant, 3K Metallurgov Ave., Podolsk, Moscow Oblast 142155, Russia) and, personally, the CEO Andrey G. Tsydenov for providing aluminum samples with PEO coatings for this study.

Conflicts of Interest: The authors declare no conflicts of interest.

References

1. Shin, J.; Kim, T.; Kim, D.E.; Kim, D.; Kim, K. Castability and mechanical properties of new 7xxx aluminum alloys for automotive chassis/body applications. *J. Alloys Compd.* **2017**, *698*, 577–590. [CrossRef]
2. Akopyan, T.K.; Belov, N.A. Approaches to the design of the new high-strength casting aluminum alloys of 7xxx series with high iron content. *Non Ferr. Met.* **2016**, *1*, 20–27. [CrossRef]
3. Mann, V.K.; Alabin, A.N.; Krokhin, A.Y.; Frolov, A.V.; Belov, N.A. New Generation of High Strength Aluminum Casting Alloys. *Light Met. Age* **2015**, *73*, 44–47.
4. Shurkin, P.K.; Belov, N.A.; Musin, A.F.; Aksenov, A.A. Novel High-Strength Casting Al−Zn−Mg−Ca−Fe Aluminum Alloy without Heat Treatment. *Russ. J. Non-Ferr. Met.* **2020**, *61*, 179–187. [CrossRef]
5. Gamin, Y.V.; Belov, N.A.; Akopyan, T.K.; Timofeev, V.N.; Cherkasov, S.O.; Motkov, M.M. Effect of Radial-Shear Rolling on the Structure and Hardening of an Al–8%Zn–3.3%Mg–0.8%Ca–1.1%Fe Alloy Manufactured by Electromagnetic Casting. *Materials* **2023**, *16*, 677. [CrossRef] [PubMed]
6. Shurkin, P.K.; Akopyan, T.K.; Galkin, S.P.; Aleshchenko, A.S. Effect of radial shear rolling on the structure and mechanical properties of a new-generation high-strength aluminum alloy based on the Al-Zn-Mg-Ni-Fe system. *Met. Sci. Heat Treat.* **2019**, *60*, 11–12. [CrossRef]
7. Shurkin, P.; Akopyan, T.; Korotkova, N.; Prosviryakov, A.; Bazlov, A.; Komissarov, A.; Moskovskikh, D. Microstructure and Hardness Evolution of Al8Zn7Ni3Mg Alloy after Casting at very Different Cooling Rates. *Metals* **2020**, *10*, 762. [CrossRef]
8. Rakoch, A.G.; Gladkova, A.A.; Dub, A.V. *Plasma Electrolytic Treatment of Aluminum and Titanium Alloys*; MISiS PH: Moscow, Russia, 2017; pp. 8–27.
9. Zhu, L.; Guo, Z.; Zhang, Y.; Li, Z.; Sui, M. A mechanism for the growth of a plasma electrolytic oxide coating on Al. *Electrochim. Acta* **2016**, *208*, 296–303. [CrossRef]
10. Letyagin, N.V.; Sokorev, A.A.; Kokarev, V.N.; Shatrov, A.S.; Tsydenov, A.G.; Finogeev, A.S.; Musin, A.F.; Petrzhik, M.I. The comparative characteristics of the structure and functional properties of coatings formed on aluminum alloys 2xxx and 7xxx series by the method of plasma electrolytic oxidation. *Phys. Met. Metallogr.* **2023**, *124*, 238–244. [CrossRef]
11. Zhang, J.; Dai, W.; Wang, X.; Wang, Y.; Yue, H.; Li, Q.; Yang, X.; Guo, C.; Li, C. Micro-arc oxidation of Al alloys: Mechanism, microstructure, surface properties, and fatigue damage behavior. *J. Mater. Res. Technol.* **2023**, *23*, 4307–4333. [CrossRef]
12. Rodriguez, L.; Paris, J.-Y.; Denape, J.; Delbé, K. Micro-Arcs Oxidation Layer Formation on Aluminium and Coatings Tribological Properties—A Review. *Coatings* **2023**, *13*, 373. [CrossRef]
13. Liu, C.; Wang, Q.; Cao, X.; Cha, L.; Ye, R.; Ramachandran, C.S. Significance of plasma electrolytic oxidation treatment on corrosion and sliding wear performances of selective laser melted AlSi10Mg alloy. *Mater. Charact.* **2021**, *181*, 111479. [CrossRef]
14. Wang, P.; Wu, T.; Xiao, Y.T.; Zhang, L.; Pu, J.; Cao, W.J.; Zhong, X.M. Characterization of micro-arc oxidation coatings on aluminum drill pipes at different current density. *Vacuum* **2017**, *142*, 21–28. [CrossRef]
15. Cerchier, P.; Pezzato, L.; Gennari, C.; Moschin, E.; Moro, I.; Dabal, M. PEO coating containing copper: A promising anticorrosive and antifouling coating for seawater application of AA 7075. *Surf. Coat. Technol.* **2020**, *393*, 125774. [CrossRef]
16. Zhu, M.; Song, Y.; Liu, Z.; Xu, D.; Dong, K.; Han, E.H. Optimization of thermal control and corrosion resistance of PEO coatings on 7075 aluminum alloy by frequency alteration. *Surf. Coat. Technol.* **2022**, *446*, 128797. [CrossRef]

17. Lu, C.; Ding, J.; Shi, P.; Jia, J.; Xie, E.; Sun, Y. Effects of Texture Density on the Tribological Properties of Plasma Electrolytic Oxidation/Polytetrafluoroethylene Coatings Formed on Aluminum Alloys. *Macromol. Mater. Eng.* **2022**, *307*, 2100678. [CrossRef]
18. Li, K.; Zhang, G.; Chen, K.; Li, W.; Zhu, Z.; Huang, Y.; Zhu, W.; Liao, Z.; Wan, B.; Liang, J.; et al. Effects of Ni content on microstructure and performance of MAO coatings on binary Al–Ni alloys. *J. Mater. Res. Technol.* **2024**, *28*, 3597–3608. [CrossRef]
19. Famiyeh, L.; Huang, X. Plasma Electrolytic Oxidation Coatings on Aluminum Alloys: Microstructures, Properties, and Applications. *Mod. Concept. Mater. Sci.* **2019**, *2*, 000526.
20. Wang, C.; Ma, R.; Du, A.; Fan, Y.; Zhao, X.; Cao, X. Growth methods of PEO coatings on 7075 aluminum alloy at two cathodic current densities. *Surf. Coat. Technol.* **2022**, *432*, 128099. [CrossRef]
21. Tillous, K.; Toll-Duchanoy, T.; Bauer-Grosse, E.; Hericher, L.; Geandier, G. Microstructure and phase composition of microarc oxidation surface layers formed on aluminium and its alloys 2214-T6 and 7050-T74. *Surf. Coat. Technol.* **2009**, *203*, 2969–2973. [CrossRef]
22. Ghafaripoora, M.; Raeissia, K.; Santamariab, M.; Hakimizada, A. The corrosion and tribocorrosion resistance of PEO composite coatings containing α-Al_2O_3 particles on 7075 Al alloy. *Surf. Coat. Technol.* **2018**, *349*, 470–479. [CrossRef]
23. Premchand, C.; Manojkumar, P.; Lokeshkumar, E.; Rama Krishna, L.; Ravisankar, B.; Rameshbabu, N. Surface characteristics of AC PEO coatings fabricated on commercial Al alloys. *Surf. Coat. Technol.* **2022**, *449*, 128975. [CrossRef]
24. Oh, Y.-J.; Mun, J.-I.; Kim, J.-H. Effects of alloying elements on microstructure and protective properties of Al_2O coatings formed on aluminum alloy substrates by plasma electrolysis. *Surf. Coat. Technol.* **2009**, *204*, 141–148. [CrossRef]
25. Gulec, A.E.; Gencer, Y.; Tarakci, M. The characterization of oxide based ceramic coating synthesized on Al-Si binary alloys by microarc oxidation. *Surf. Coat. Technol.* **2015**, *269*, 100–107. [CrossRef]
26. Li, K.; Li, W.; Zhang, G.; Zhu, W.; Zheng, F.; Zhang, D.; Wang, M. Effects of Si phase refinement on the plasma electrolytic oxidation of eutectic Al-Si alloy. *J. Alloys Compd.* **2019**, *790*, 650–656. [CrossRef]
27. Rogov, A.B.; Lyu, H.; Matthews, A.; Yerokhin, A. AC plasma electrolytic oxidation of additively manufactured and cast AlSi12 alloys. *Surf. Coat. Technol.* **2020**, *399*, 126116. [CrossRef]
28. Mora-Sanchez, H.; Olmo, R.; Rams, J.; Torres, B.; Mohedano, M.; Matykina, E.; Arrabal, R. Hard Anodizing and Plasma Electrolytic Oxidation of an Additively Manufactured Al-Si alloy. *Surf. Coat. Technol.* **2021**, *420*, 127339. [CrossRef]
29. Cengiz, S. Synthesis of eutectic Al–18Ce alloy and effect of cerium on the PEO coating growth. *Mater. Chem. Phys.* **2020**, *247*, 122897. [CrossRef]
30. Letyagin, N.V.; Akopyan, T.K.; Sokorev, A.A.; Sviridova, T.A.; Cherkasov, S.O.; Mansurov, Y.N. The Characterization of Coatings Formed on As-Cast Al, Al–Si, and Al–Ca Aluminum Substrates by Plasma Electrolytic Oxidation. *Metals* **2023**, *13*, 1509. [CrossRef]
31. Tarakci, M. Plasma electrolytic oxidation coating of synthetic Al-Mg binary alloys. *Mater. Char.* **2011**, *62*, 1214–1221. [CrossRef]
32. Gencer, Y.; Gulec, A.E. The effect of Zn on the microarc oxidation coating behavior of synthetic Al-Zn binary alloys. *J. Alloys Compd.* **2012**, *525*, 159–165. [CrossRef]
33. Oter, Z.C.; Gencer, Y.; Tarakci, M. The characterization of the coating formed by Microarc oxidation on binary Al-Mn alloys. *J. Alloys Compd.* **2015**, *650*, 185–192. [CrossRef]
34. Cengiz, S.; Tarakci, M.; Gencer, Y.; Devecili, A.O.; Azakli, Y. Oxide based ceramic coating on Al-4Cu alloy by microarc oxidation. *Acta Phys. Pol. A* **2013**, *123*, 445–448. [CrossRef]
35. Agureev, L.; Savushkina, S.; Ashmarin, A.; Borisov, A.; Apelfeld, A.; Anikin, K.; Tkachenko, N.; Gerasimov, M.; Shcherbakov, A.; Ignatenko, V.; et al. Study of Plasma Electrolytic Oxidation Coatings on Aluminum Composites. *Metals* **2018**, *8*, 459. [CrossRef]
36. Kwon, S.Y.; Shin, D.; Michi, R.A.; Poplawsky, J.D.; Wang, H.; Yang, Y.; Bahl, S.; Shyam, A.; Plotkowski, A. Effect of microalloying additions on microstructural evolution and thermal stability in cast Al-Ni alloys. *J. Alloys Compd.* **2024**, *997*, 174810. [CrossRef]
37. Czerwinski, F.; Aniolek, M.; Li, J. Strengthening retention and structural stability of the Al-Al_3Ni eutectic at high temperatures. *Scr. Mater.* **2022**, *214*, 114679. [CrossRef]
38. Deng, J.W.; Chen, C.; Liu, X.C.; Li, Y.P.; Zhoua, M.; Guo, S.M. A high-strength heat-resistant Al-5.7Ni eutectic alloy with spherical Al_3Ni nanoparticles by selective laser melting. *Scripta Mater.* **2021**, *203*, 114034. [CrossRef]
39. Cosan, K.A.; Gunduz, K.O.; Tarakcı, M.; Gencer, Y. Plasma electrolytic oxidation of as-cast and heat-treated binary Al-Ni alloys. *Surf. Coat. Technol.* **2022**, *450*, 128998. [CrossRef]
40. Shelekhov, E.V.; Sviridova, T.A. Programs for X-ray analysis of polycrystals. *Met. Sci. Heat Treat.* **2000**, *42*, 309–313. [CrossRef]
41. *ASTM G99-17*; Standard Test Method for Wear Testing with a Pin-on-Disk Apparatus. ASTM: West Conshohocken, PA, USA, 2017.
42. *ISO 4287-2014*; Geometrical Product Specifications (GPS). Surface Texture. Profile Method. Terms, Definitions and Surface Texture Pa-rameters. Standartinform: Moscow, Russia, 2015.
43. Ikeuba, A.I.; Zhang, B.; Wang, J.; Han, E.-H.; Ke, W.; Okafor, P.C. SVET and SIET Study of Galvanic Corrosion of Al/$MgZn_2$ in Aqueous Solutions at Different pH. *J. Electrochem. Soc.* **2018**, *165*, 180–194. [CrossRef]
44. Shi, J.; Mu, Y.; Shen, H.; Xing, N. Effect of Zn on Corrosion Resistance of 5083 Alloys. *J. Phys. Conf. Ser.* **2023**, *2468*, 012018. [CrossRef]